MODELLING OF OPEN-CELL CELLULAR SOLIDS AT FINITE DEFORMATIONS

Per Hård af Segerstad, Ragnar Larsson and Staffan Toll

Department of Applied Mechanics
Chalmers University of Technology
41296 Göteborg, Sweden
Toll@Chalmers.se

ABSTRACT

We present a thermodynamically consistent, mechanistic approach for modelling the inelastic response of open cell foams at large strains. The cellular solid is considered as a network of struts. The struts are described as elastic at small strains and buckle plastically beyond a critical strain. Our description of the strut response requires only a scalar valued response function, which facilitates the introduction of multiple nonlinear mechanisms, such as hyperelasto-viscoplasticity and damage. An additional hyperelastic volumetric response is introduced to capture the stiff response near the point-of-compaction. The model is implemented in the FEM code ABAQUS. Experiments are done for an open-cell aluminium foam. All material parameters are determined by a simple compression test, and subsequently used to simulate the indentation of a rigid sphere into a foam cylinder. The model accurately captures the experimental load-displacement relation and the deformed geometry.

1 INTRODUCTION

Although cellular solids are fairly well described in the literature at small elastic deformations, cf. Gibson and Ashby (1997), their inelastic behaviour and large deformations is not as well understood. The cell structure exhibits complex deformation mechanisms, resulting in a highly non-linear macroscopic behaviour. Three different regimes can usually be identified, see Fig. 1. Region I is approximately linear elastic and primarily governed by small deflection bending of struts. At a critical point, struts loaded in compression lose stability and buckle, elastically or plastically. Thus with increasing deformation, the number of collapsed struts increases, and the overall stiffness decreases. This progressive microbuckling gives rise to a plateau in region II. Finally in region III, the struts can no longer deflect freely but pack together by contact, towards the point-of-compaction.

For hyperelastic response, Zilauts and Lagzdin (1992) developed a mechanistic model based on a single-strut cell with affine motion of the strut endpoints. This model allows for finite deformations, including strut re-orientation and buckling. A hyperelastic model by Hård af Segerstad and Toll (2008) was based on a similar idea. Warren and Kraynik (1991) and Wang and Cuitiño (2000) based their hyperelastic models on affine motion of strut midpoints rather than endpoints for a unit-cell consisting of four struts.

For inelastic response, few mechanistic models have been proposed. Zhang and Lee (2003) modelled a cubic unit cell with a rigid-plastic material model, but only at small strains. Hård af Segerstad et al. (2008) presented a finite strain based

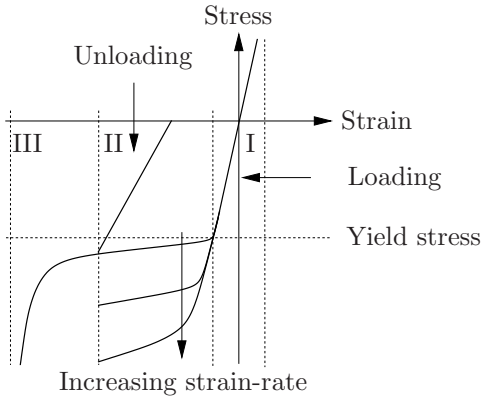

Figure 1: Schematic response to large uniaxial compressive deformation of a cellular solid. Regime I—linear elasticity; regime II—plateau; regime III—densification. The effects of strain-rate and damage (reduction of elastic stiffness), on the unloading curve, are also illustrated.

constitutive model including plasticity, viscoplasticity, hardening/softening, damage and deformation induced anisotropy.

The objective of the present work is to develop an ineastic model, suitable for finite element (FEM) computations. The aim is to capture the complete response, and to model the most important mechanisms on the level of individual struts. Plastic buckling is thus modelled by 1D viscoplasticity on the strut level, and stiffness reduction due to the formation of plastic hinges is modelled by 1D damage mechanics, on the strut level.

2 MODEL

The microstructure is considered as a network of connected struts, Fig. 2. Regimes I and II where the struts deflect freely, will be modelled mechanistically on the strut level, while regime III will be modelled macroscopically. We thus introduce a free energy density (per unit undeformed volume) which is subdivided into a *stretch energy* due to the change of distance between strut vertices, and a macroscopic *compaction energy* $\bar{\Psi}_0^{\mathrm{c}}$ due to the crowding of struts near the *point-of-compaction*:

$$\bar{\Psi}_0 = \frac{1}{v_{\bar{\Omega}_0}} \sum_{i=1}^{N_{\bar{\Omega}_0}} v_{0i} \Psi_{0i}^{\mathrm{s}}(\lambda_i, \mathcal{Q}_i), + \bar{\Psi}_0^{\mathrm{c}}(\bar{J}), \tag{1}$$

where Ψ_{0i}^{s} is the stretch energy of a strut i, λ_i is the stretch of the strut, $\mathcal{Q}_i$ is a set of internal variables for the strut, v_{0i} is the volume of the strut, $N_{\bar{\Omega}_0}$ is the number of struts in a region $\bar{\Omega}_0$, $v_{\bar{\Omega}_0}$ is the volume of $\bar{\Omega}_0$ and $\bar{J}$ is the macroscopic volume ratio.

The Clausius-Planck inequality, in terms of the second Piola-Kirchhoff stress $\bar{\mathbf{S}}$

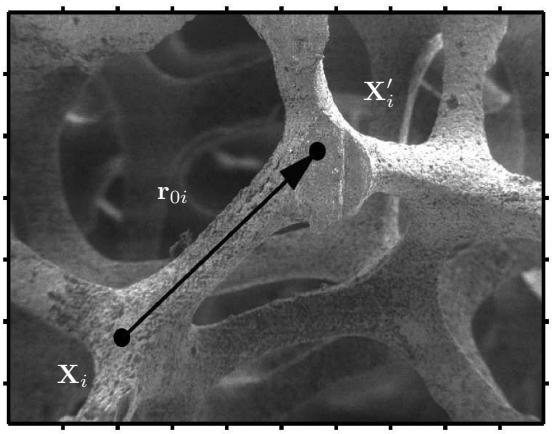

Figure 2: Strut vertices $\mathbf{X}'_i$, $\mathbf{X}_i$ and *vertex-to-vertex* vector $\mathbf{r}_{0i}$ in the microstructure of an aluminium foam (Duocel 6101-0, 40 ppi).

becomes

$$\begin{aligned}\frac{1}{2}\bar{\mathbf{S}} : \dot{\bar{\mathbf{C}}} - \dot{\bar{\Psi}}_0 &= \left(\bar{\mathbf{S}} - \frac{2}{v_{\bar{\Omega}_0}} \sum_{i=1}^{N_{\bar{\Omega}_0}} v_{0i} \frac{\partial \Psi^{\mathrm{s}}_{0i}}{\partial \lambda_i} \frac{\partial \lambda_i}{\partial \bar{\mathbf{C}}} - 2 \frac{\partial \bar{\Psi}^{\mathrm{c}}_0}{\partial \bar{J}} \frac{\partial \bar{J}}{\partial \bar{\mathbf{C}}} \right) : \dot{\bar{\mathbf{C}}} \\ &- 2 \frac{1}{v_{\bar{\Omega}_0}} \sum_{i=1}^{N_{\bar{\Omega}_0}} v_{0i} \frac{\partial \Psi^{\mathrm{s}}_{0i}}{\partial \Omega_i} \dot{\Omega}_i \geq 0, \end{aligned} \tag{2}$$

where $\bar{\mathbf{C}}$ is the right Cauchy-Green deformation tensor. This yields the Coleman-Noll constitutive equation for the overall second Piola-Kirchhoff stress,

$$\bar{\mathbf{S}} = \frac{2}{v_{\bar{\Omega}_0}} \sum_{i=1}^{N_{\bar{\Omega}_0}} v_{0i} \frac{\partial \Psi^{\mathrm{s}}_{0i}}{\partial \lambda_i} \frac{\partial \lambda_i}{\partial \bar{\mathbf{C}}} + 2 \frac{\partial \bar{\Psi}^{\mathrm{c}}_0}{\partial \bar{J}} \frac{\partial \bar{J}}{\partial \bar{\mathbf{C}}}, \tag{3}$$

and the dissipation inequality

$$- \sum_{i=1}^{N_{\bar{\Omega}_0}} \frac{\partial \Psi^{\mathrm{s}}_{0i}}{\partial \Omega_i} \dot{\Omega}_i \geq 0. \tag{4}$$

It now remains to specify the free energy functions $\Psi^{\mathrm{s}}_{0i}(\lambda_i, \Omega_i)$ and $\bar{\Psi}^{\mathrm{c}}_0(\bar{J})$, the stretch relation $\partial \lambda_i / \partial \bar{\mathbf{C}}$ and the set of internal state variables Ω_i, subject to Eq. (4).

2.1 Stretch contribution

Following Hård af Segerstad et al. (2008), we introduce the strut *vertex-to-vertex* vector in the material configuration,

$$\mathbf{r}_{0i} := \mathbf{X}'_i - \mathbf{X}_i = r_{0i} \mathbf{N}_i, \tag{5}$$

where $\mathbf{X}'_i$ and $\mathbf{X}_i$ are the strut vertex points, see Fig. 2, r_{0i} is the strut length and $\mathbf{N}_i$ is the strut (reference) director ($\| \mathbf{N}_i \| = 1$). The evolution of the material strut

vector $\mathbf{r}_{0i}$ is modelled by the *affine* assumption:

$$\mathbf{r}_i = \bar{\mathbf{F}} \cdot \mathbf{r}_{0i} = r_{0i} \bar{\mathbf{F}} \cdot \mathbf{N}_i, \tag{6}$$

where $\bar{\mathbf{F}}$ is the macroscopic deformation gradient tensor. It follows from Eqs. (5) and (6) that the current orientation and stretch of a strut i are

$$\mathbf{n}_i = \lambda_i^{-1} \bar{\mathbf{F}} \cdot \mathbf{N}_i, \qquad \text{and} \qquad \lambda_i = r_i / r_{0i} = \left(\mathbf{N}_i \cdot \bar{\mathbf{C}} \cdot \mathbf{N}_i \right)^{1/2} \tag{7}$$

Next, we introduce the multiplicative elastic-plastic decomposition of the macroscopic deformation gradient, $\bar{\mathbf{F}} = \bar{\mathbf{F}}^{\mathrm{e}} \cdot \bar{\mathbf{F}}^{\mathrm{p}}$, cf. Lee (1969), which leads to a multiplicative split of the microscopic stretch

$$\lambda_i = \lambda_i^{\mathrm{e}} \lambda_i^{\mathrm{p}}. \tag{8}$$

To facilitate the treatment of dissipative mechanisms, we introduce the *logarithmic strains*: $\varepsilon_i := \log(\lambda_i)$, $\varepsilon_i^{\mathrm{e}} := \log(\lambda_i^{\mathrm{e}})$ and $\varepsilon_i^{\mathrm{p}} := \log(\lambda_i^{\mathrm{p}})$ leading to the additive split

$$\varepsilon_i = \varepsilon_i^{\mathrm{e}} + \varepsilon_i^{\mathrm{p}}. \tag{9}$$

We choose the internal variables as $\mathcal{Q}_i := \{\varepsilon_i^{\mathrm{p}}, \kappa_i, \alpha_i\}$ and make the following ansatz for the *stretch energy* function of the individual struts:

$$\Psi_{0i}^{\mathrm{s}} = \frac{1}{2} \left((1 - \alpha_i) k_i (\varepsilon_i - \varepsilon_i^{\mathrm{p}})^2 + H_i \kappa_i^2 \right). \tag{10}$$

In Eq. (10) α_i is a damage parameter and k_i is an elastic modulus, H_i is the hardening/softening modulus and κ_i is the drag-stress. The resulting material time derivative of $\bar{\Psi}_{0i}^{\mathrm{s}}$ is obtained as

$$\dot{\Psi}_{0i}^{\mathrm{s}}(\varepsilon_i, \varepsilon_i^{\mathrm{p}}, \kappa_i, \alpha_i) \;=\; \frac{\partial \Psi_{0i}^{\mathrm{s}}}{\partial \varepsilon_i} \dot{\varepsilon}_i + \frac{\partial \Psi_{0i}^{\mathrm{s}}}{\partial \varepsilon_i^{\mathrm{p}}} \dot{\varepsilon}_i^{\mathrm{p}} + \frac{\partial \Psi_{0i}^{\mathrm{s}}}{\partial \kappa_i} \dot{\kappa}_i + \frac{\partial \Psi_{0i}^{\mathrm{s}}}{\partial \alpha_i} \dot{\alpha}_i. \tag{11}$$

It remains to choose the evolution equations for $\varepsilon_i^{\mathrm{p}}$, κ_i and α_i such that Eq. (4) is satisfied. Hence the present approach guarantees that the dissipation inequality is satisfied at all times on the microlevel, and the resulting model is therefore thermodynamically consistent.

Further, we introduce the effective microscopic Kirchhoff stress $\tilde{\tau}$:

$$\tilde{\tau}_i = \frac{\tau_i}{1 - \alpha_i} = k_i (\varepsilon_i - \varepsilon_i^{\mathrm{p}}), \tag{12}$$

and define the drag stress $\mathcal{K}_i$ and damage force $\mathcal{A}_i$ as

$$\mathcal{K}_i := -\frac{\partial \Psi_{0i}^{\mathrm{s}}}{\partial \kappa_i} = -H_i \kappa_i, \quad \mathcal{A}_i := -\frac{\partial \Psi_{0i}^{\mathrm{s}}}{\partial \alpha_i} = \frac{1}{2} k_i (\varepsilon_i - \varepsilon_i^{\mathrm{p}})^2 = \frac{1}{2 k_i} \tilde{\tau}_i^2. \tag{13}$$

Finally we introduce the scalar valued yield function Φ_i and inelastic potential Φ_i^{p} on the strut level as

$$\Phi_i = -\tilde{\tau}_i - \tau_{\mathrm{y}i} - \mathcal{K}_i, \quad \Phi_i^{\mathrm{P}} = \Phi_i + \frac{1}{2} \frac{\mathcal{A}_i^2}{S_i (1 - \alpha_i)^m}, \tag{14}$$

where the damage modulus, S_i, is a (scalar) material parameter and the damage exponent m governs the rate of damage evolution. The expression for the yield

function Φ_i, cf. Eq. (14), is motivated by observations from Zhou et al. (2004) and Kim and Al-Hassani (2002) who investigated the microstructural deformation of open-cell aluminium foams. The inelastic potential Φ_i^{P} is quadratic in $\mathcal{A}_i$ and thus thermodynamically consistent. To account for the evolution of rate-dependent viscoplastic flow and damage, while satisfying Eq. (4), we formulate the evolution of the inelastic variables $\varepsilon_i^{\mathrm{p}}, \kappa_i$ and α_i according to Perzyna (1966) and Lemaitre and Chaboche (1990):

$$\dot{\varepsilon}_i^{\mathrm{p}} = \frac{1}{t_\star}\eta(\Phi_i)\frac{\partial \Phi_i^{\mathrm{P}}}{\partial \tau_i} = \frac{1}{t_\star(1-\alpha_i)}\eta(\Phi_i)\frac{\partial \Phi_i^{\mathrm{P}}}{\partial \tilde{\tau}_i} = \frac{1}{t_\star(1-\alpha_i)}\eta(\Phi_i)\mathrm{sign}(\tilde{\tau}_i), \tag{15}$$

$$\dot{\kappa}_i = \frac{1}{t_\star}\eta(\Phi_i)\frac{\partial \Phi_i^{\mathrm{P}}}{\partial \mathcal{K}_i} = -\frac{1}{t_\star}\eta(\Phi_i), \tag{16}$$

$$\dot{\alpha}_i = \frac{1}{t_\star}\eta(\Phi_i)\frac{\partial \Phi_i^{\mathrm{P}}}{\partial \mathcal{A}_i} = \frac{1}{2t_\star k_i S_i(1-\alpha_i)^m}\eta(\Phi_i)\tilde{\tau}_i^2 \geq 0, \tag{17}$$

where $t_\star$ is the relaxation time, $\eta(\Phi_i)$ is a Norton type overstress function,

$$\eta(\Phi_i) := \left(\frac{|\Phi_i| + \Phi_i}{2\tau_{\mathrm{ci}}}\right)^n, \tag{18}$$

and n is the creep exponent.

Equations (12)-(18) together with Eq. $(7)_2$ determine the stretch energy Ψ_{0i}^{s} and may be solved by, e.g., implicit Backward Euler integration.

2.2 Compaction contribution

We propose a volumetric free energy function for the compaction behaviour of the following form:

$$\bar{\Psi}_0^{\mathrm{c}} = \mathcal{C}\left(\bar{J} - \frac{3(\phi_0-1)^2}{\bar{J}-\phi_0} - \frac{(\phi_0-1)^3}{2(\bar{J}-\phi_0)^2} + 3\,(\phi_0-1)\log(\bar{J}-\phi_0)\right) + \mathcal{C}_0, \tag{19}$$

$$\mathcal{C}_0 = -\frac{1}{2}\mathcal{C}\left((5+6\log(1-\phi_0))\phi_0 - 6\log(1-\phi_0) - 3\right), \tag{20}$$

where $\mathcal{C}$ is a scalar valued compaction modulus and ϕ_0 is the initial volume fraction of solid material. This compaction energy function has the desired property that it is negligible in the regions I-II, where mutual contacts between the struts are insignificant, while compression near the *point-of-compaction* is penalised, as $\bar{\Psi}^{\mathrm{c}} \to \infty$ whenever the pore-space $\phi^{\mathrm{p}} \to 0$, corresponding to $\bar{J} = \phi_0$. It is strictly convex and has a minimum which is zero for $\bar{J} = 1$. This simple contribution prevents negative volumes in the FEM solution scheme, since highly volumetric deformed elements become infinitely stiff, and thereby significantly improves stability of the iterative solution.

2.3 Constitutive equation

Introducing Eqs. (10) and (19) into Eq. (1) yields the closed form for the total second Piola-Kirchhoff stress:

$$\bar{\mathbf{S}} = \frac{\phi_0}{N}\sum_{i=1}^{N}(1-\alpha_i)k_i(\varepsilon_i - \varepsilon_i^{\mathrm{p}})\exp(-2\varepsilon_i)\mathbf{N}_i \otimes \mathbf{N}_i + \bar{J}\mathcal{C}\left(\frac{\bar{J}-1}{\bar{J}-\phi_0}\right)^3 \bar{\mathbf{C}}^{-\mathrm{T}}. \tag{21}$$

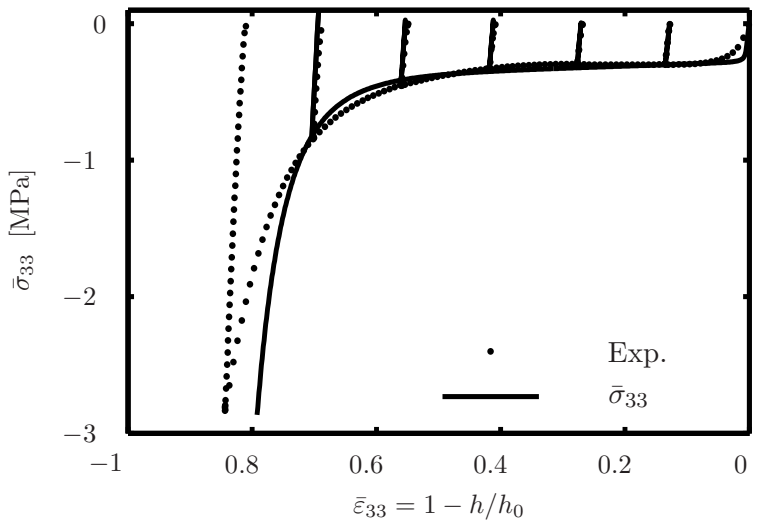

Figure 3: Calibration test (compression between parallel plates, cyclic loading/unloading): model (-); experiment ($\cdots$).

Here ergodicity is assumed, in the sense that the average over a representative volume $v_{\bar{\Omega}_0}$ may be replaced by an average taken over a finite representative set of N struts. We characterise the struts, statistically, by their orientations $\mathbf{N}_i$ alone, assuming that other strut properties are uncorrelated with $\mathbf{N}_i$. Thereby the set of N struts in Eq. (21) reduces to a set of N directors $\{\mathbf{N}_1, \mathbf{N}_2, \ldots \mathbf{N}_{N-1}, \mathbf{N}_N\}$.

3 EXPERIMENTAL

An aluminium foam (Duocel 6101-0, 40ppi) with relative density $0.039 \leq \rho^* \leq 0.048$ was studied, cf. Fig. 2.

To identify the quasi-static set of material parameters: $\mathcal{S} := \{k, \tau_y, H, \mathcal{C}_0\}$, only stress-strain data in compression are needed. To perform the calibration experiments the Duocel foam was cut into cylindrical discs having a height $h_0 = 15.0$mm and diameter $2a = 150.0$mm. Thus the height to diameter was kept small to minimize the influence of the free boundary, yet the height was large compared to the cell size. The disc specimens were confined between two horizontal parallel plates in a tensile tester, and then deformed by imposing a vertical motion $-\dot{h} = 0.001$m/s on the upper plate while recording displacement and force.

As a structural test, a steel hemisphere was pressed with a constant velocity $-\dot{d} = 0.001$m/s into cylindrical foam specimens with height $h_1 = 100$mm and radius $a = 75$mm.

4 SIMULATION

The constitutive equation (21) was linearised and implemented as a user-defined subroutine in the FEM software ABAQUS standard. Thus, the experiments described above were simulated using the constitutive model and a fixed set of 100 isotropically distributed strut directors $\{\mathbf{N}_i\}$. The model parameters $\mathcal{S}$ were first estimated from the calibration experiment. Then the indentation test was simulated, holding

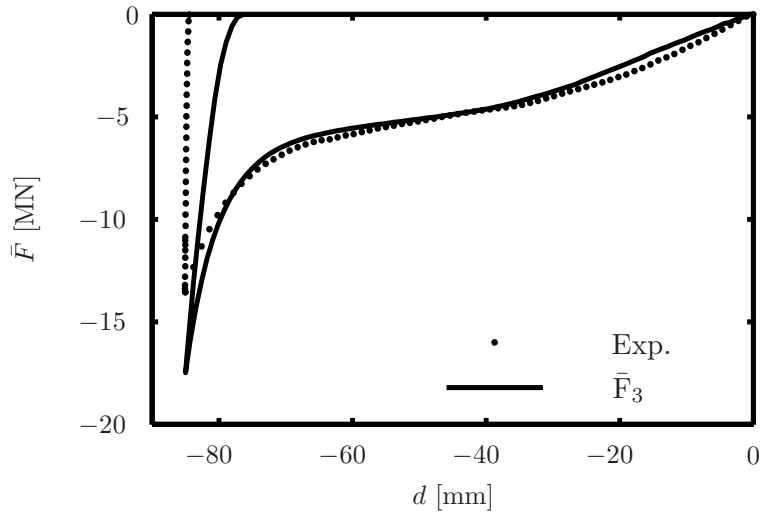

Figure 4: Indentation test: prediction (-); experiment ($\cdots$).

$\mathcal{S}$ fixed. The predicted force ($\bar{F}$) versus indentation depth (d) is plotted in Fig. 4. The simulated deformation, at different indentation depths, is shown in Fig. 5 and a comparison between the predicted and experimental deformations is shown in Fig. 6.

5 CONCLUSIONS

The approach to model structural cellular solids based on a 1-dimensional strut response and affine motion of strut vertices (in the non-linear regime) appears to work well.

The affine assumption together with the 1-dimensional modelling on the strut level shortens the computational time substantially and ensures numerical stability.

The 1-dimensional constitutive modelling on the micro level makes it easy to incorporate multiple dissipative mechanisms, such as plasticity/viscoplasticity, hardening/softening and damage. It should also be straightforward to introduce other types of behaviour in the same fashion. The technique automatically accounts for deformation induced anisotropy.

The compaction (Region III) response was modelled macroscopically, penomenologically, by a hyperelastic volumetric contribution. This response is the simplest reasonable, with no mechanistic basis whatever.

The model was successfully implemented in ABAQUS. Experiments on the indentation of a rigid sphere into a block of aluminium foam were well predicted, all model parameters being determined by one simple compression test.

ACKNOWLEDGEMENT

This work was financed by the vehicle research program (ffp) and the following participating companies: Finnveden AB, Gestamp HardTech AB, Outokumpu Stainless AB, SAAB Automobile AB, Volvo AB, Volvo Car Corporation.

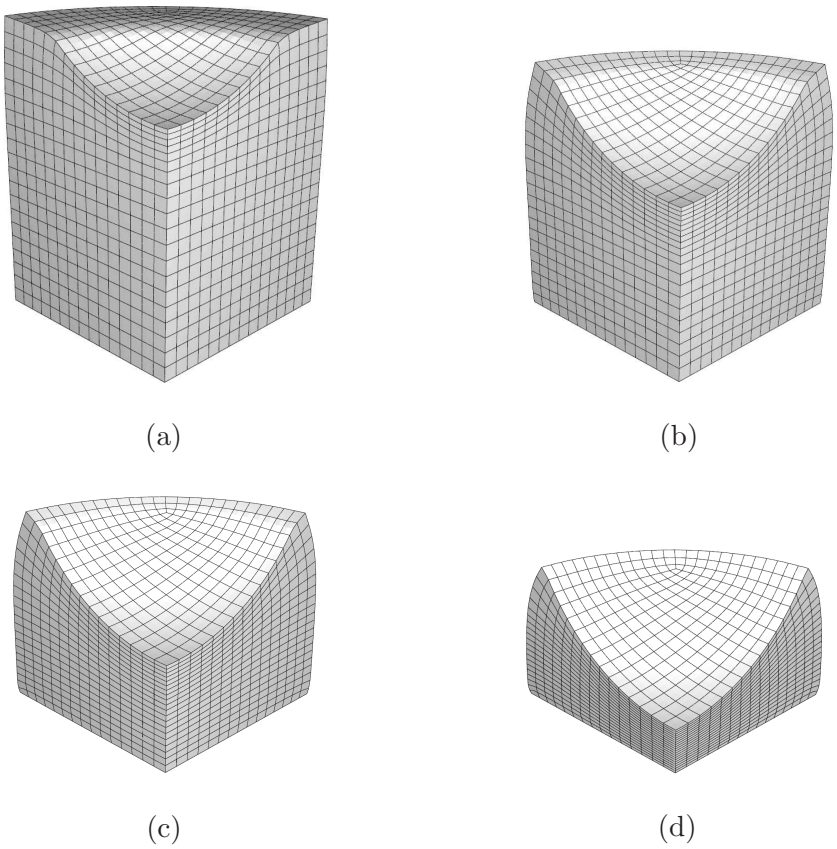

Figure 5: Simulation of indentation test. (a) 25%, (b) 50%, (c) 75%, (d) 100% of total indentation.

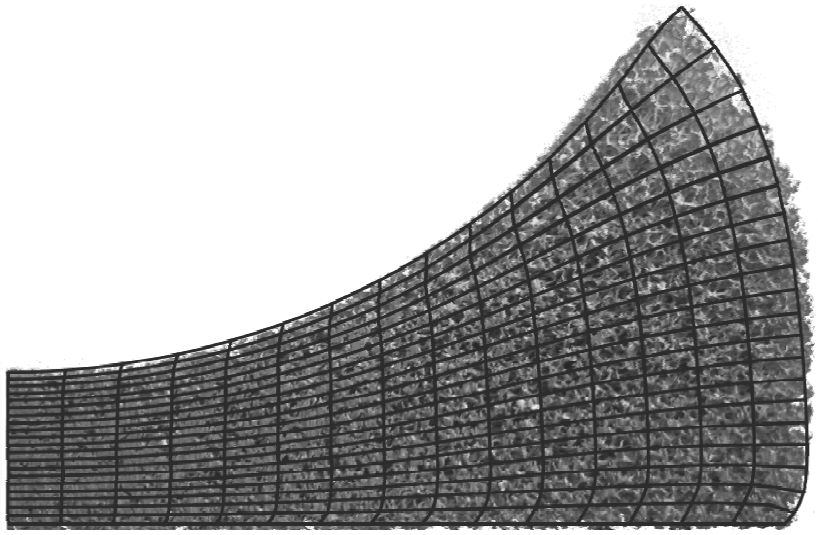

Figure 6: Comparison between predicted and experimental deformed shape.

References

Gibson, L. J. and Ashby M. F. 1997. Cellular solids Structure & properties. Cambridge University Press, Cambridge.

Hård af Segerstad, P. and Toll, S., 2008. Open-cell cellular solids: A constitutive equation for hyperelasticity with deformation induced anisotropy. International Journal of Solids and Structures. 45, 1978–1992.

Hård af Segerstad, Larsson, R. and Toll, S. 2008. A constitutive equation for open-cell cellular solids, including viscoplasticity, damage and deformation induced anisotropy. International Journal of Plasticity. 24, 896–914.

Kim, H. S. and Al-Hassani S. T. S. 2002. The effect of doubly tapered strut morphology on the plastic yield surface of cellular materials. International Journal of Mechanical Science. 44, 1559–1581.

Lee, E. H. 1969. Elastic-plastic deformations at finite strains. Journal of Applied Mechanics. 36, 1–6.

Lemaitre, J. and Chaboche, J.-L. 1990. Mechanics of Solid Materials. Cambridge University Press.

Perzyna, P. 1966. Fundamental problems in viscoplasticity. Avd Appl Mech. 9, 243–377.

Wang, Y. and Cuitiño, A. M. 2000. Three-dimensional nonlinear open-cell foams with large deformations. Journal of the Mechanics and Physics of Solids. 48, 961–988.

Warren, W. E. and Kraynik, A. M. 1991. The nonlinear elastic behavior of open-cell foams. Journal of Applied Mechanics. 58, 376–381.

Zhang, J., Lee, J., 2003. A plasticity model for cellular materials with open-celled structure. International Journal of Plasticity. 19, 749–770.

Zhou, J., Shrotriya P., Soboyejo, W. O. 2004. Mechanisms and mechanics of compressive deformation in open-cell Al foams. Mechanics of Materials. 36, 781–797.

Zilauts, A. F. and Lagzdin, A. Zh. 1992. Single-bar model of cellular materials subjected to large elastic deformations. Mechanics of Composite Materials. 28, 1–7.